LOYOLA UNIVERSITY CHICAGO 1870 AD MAJOREM DEI GLORIAM eCOMMONS

Loyola University Chicago
Loyola eCommons

Chemistry: Faculty Publications and Other Works

Faculty Publications and Other Works by Department

12-22-2017

Structural Evidence of a Major Conformational Change Triggered by Substrate Binding in DapE Enzymes: Impact on the Catalytic Mechanism

Boguslaw Nocek
Midwest Center for Structural Genomics and Structural Biology

Cory Reid
Loyola University Chicago

Anna Starus
Loyola University Chicago

Tahirah Heath
Loyola University Chicago

Follow this and additional works at: https://ecommons.luc.edu/chemistry_facpubs

Part of the Biochemistry Commons, Chemistry Commons, and the Structural Biology Commons

David Bienvenues

See next page for additional authors

Author Manuscript

This is a pre-publication author manuscript of the final, published article.

Recommended Citation

Nocek, Boguslaw; Reid, Cory; Starus, Anna; Heath, Tahirah; Bienvenues, David; Osipiuk, Jerzy; Jedrzeczak, Robert; Joachimiak, Andrzej; Becker, Daniel P. Ph.D.; and Holz, Richard C.. Structural Evidence of a Major Conformational Change Triggered by Substrate Binding in DapE Enzymes: Impact on the Catalytic Mechanism. Biochemistry, 57, 5: 574-584, 2017. Retrieved from Loyola eCommons, Chemistry: Faculty Publications and Other Works, http://dx.doi.org/10.1021/acs.biochem.7b01151

This Article is brought to you for free and open access by the Faculty Publications and Other Works by Department at Loyola eCommons. It has been accepted for inclusion in Chemistry: Faculty Publications and Other Works by an authorized administrator of Loyola eCommons. For more information, please contact ecommons@luc.edu.

This work is licensed under a Creative Commons Attribution-Noncommercial-No Derivative Works 3.0 License.
© American Chemical Society 2017

Authors

Boguslaw Nocek, Cory Reid, Anna Starus, Tahirah Heath, David Bienvenues, Jerzy Osipiuk, Robert Jedrzeczak, Andrzej Joachimiak, Daniel P. Becker Ph.D., and Richard C. Holz

This article is available at Loyola eCommons: https://ecommons.luc.edu/chemistry_facpubs/85

Structural Evidence for a Major Conformational Change Triggered by Substrate Binding in DapE Enzymes: Impact on the Catalytic Mechanism

Boguslaw Nocek,[1¶] Cory Reidl,[2¶] Anna Starus,[2] Tahirah Heath,[2] David Bienvenue,[3,4] Jerzy Osipiuk,[1] Robert Jedrzejczak, [1] Andrzej Joachimiak,[1] Daniel P. Becker,[2*] and Richard C. Holz[4*]

[1]Midwest Center for Structural Genomics and Structural Biology Center, Biosciences Division, Argonne National Laboratory, Argonne, Illinois, USA, [2]The Department of Chemistry and Biochemistry, Loyola University-Chicago, 1068 W. Sheridan Rd., Chicago, IL 60626, [3]19010 33rd Ave NE, Seattle, WA 98155, [4]Department of Chemistry, Marquette University, Milwaukee, Wisconsin 53201

Running title: DapE in complex with succinate and L,L-diaminopimelic acid

Keywords: DapE, Diaminopimelate desuccinylase, M20 peptidase, SDAP-hydrolysis, Products, Enzyme conformational change, Catalysis.

¶These authors contributed equally to this work.

*Address correspondence to: Richard C. Holz, Department of Chemistry, P.O. Box 1881, Marquette University, Milwaukee, Wisconsin 53201-1881, Phone 414-288-7230, E-mail: richard.holz@marquette.edu, or Daniel P. Becker, Department of Chemistry and Biochemistry,

Loyola University-Chicago, 1068 W. Sheridan Rd., Chicago, IL 60626 Phone 773-508-3089, E-mail: dbecke3@luc.edu.

Abstract

The X-ray crystal structure of the dapE-encoded N-succinyl-L,L-diaminopimelic acid desuccinylase from *Haemophilus influenzae* (*Hi*DapE) bound by the products of hydrolysis, succinic acid and L,L-DAP, was determined at 1.95 Å. Surprisingly, the products-bound structure revealed that *Hi*DapE undergoes a significant conformational change where the catalytic domain rotates ~50 degrees and shifts ~10.1 Å (as measured at the position of the Zn atoms) relative to the dimerization domain. This heretofore unobserved closed conformation revealed significant movements within the catalytic domain compared to WT *Hi*DapE, which results in effectively closing off access to the dinuclear Zn(II) active site with the succinate carboxylate moiety bridging the dinculear Zn(II) cluster in a μ-1,3 fashion forming a bis(μ-carboxylato)dizinc(II) core with a Zn-Zn distance of 3.8 Å. Surprisingly, His194.B, which is located on the dimerization domain of the opposing chain ~10.1 Å away from the dinuclear Zn(II) active site, forms a hydrogen bond (2.9 Å) with the oxygen atom of succinic acid bound to Zn2, forming an oxyanion hole. As the closed structure forms upon substrate binding, the movement of His194.B more than ~10 Å is critical, based on site-directed mutagenesis data, for activation of the scissile carbonyl carbon of the substrate for nucleophilic attack by a hydroxide nucleophile. Employing the *Hi*DapE product-bound structure as the starting point, a reverse engineering approach called product-based transition-state modeling (PBTSM), provided structural models for each major catalytic step. These data provide insight into the catalytic reaction mechanism and also the future design of new, potent inhibitors of DapE enzymes.

Table of Contents (TOC) graphic

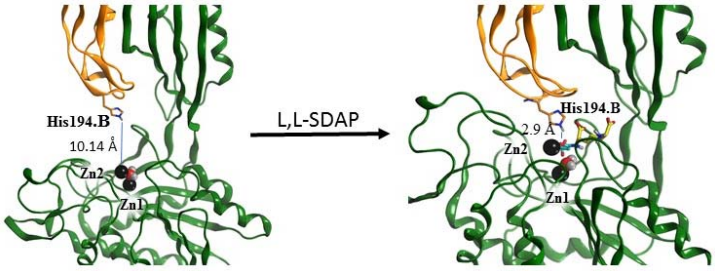

Introduction

Antimicrobial therapy has saved millions of lives over the past 80 years, yet our arsenal of effective antibiotics is increasingly diminished by the alarming rise of bacteria that are resistant to all currently available antibiotics.[1] Over two million people annually in the United States acquire infections that are resistant to antibiotics and at least 23,000 people die as a result, according to a report issued by the Centers for Disease Control and Prevention.[2] In the U.S., antibiotic resistance adds $20 billion in additional direct health care costs, with lost productivity adding an additional $35 billion annually.[3] There is an urgent need for antibacterial agents with new cellular mechanisms of action, underlying the need for research on new antimicrobialtargets with previously unexplored mechanisms of action.[4] The *meso*-diaminopimelate (mDAP)/lysine biosynthesis pathway meets these criteria as it represents unexplored, yet validated bacterial enzyme targets that are essential for bacterial viability, but are absent in mammals.

The dapE-encoded N-succinyl-L,L-diaminopimelic acid desuccinylase (DapE; EC 3.5.1.18) represents a promising bacterial enzyme target within the (mDAP)/lysine biosynthesis pathway that is essential for providing lysine and mDAP for bacterial cell wall construction in all Gram-negative and most Gram-positive bacteria.[5] It has been reported that deletion of the dapE gene in *Helicobacter pylori* and *Mycobacterium smegmatis* is lethal.[6,7] Genes encoding DapE enzymes have been identified in all pathogenic Gram-negative bacteria, and several DapE enzymes have been biochemically and structurally characterized from various bacterial sources.[8] Of particular interest are the DapEs from the "ESKAPE" pathogens, which account for more than 60% of the antibiotic resistant hospital acquired infections in the United States.[7,9,10] Alignment of the DapE gene from *Haemophilus influenzae* (*Hi*DapE) with the gene sequences of DapEs from "ESKAPE" pathogens reveals at least 49% identity.[9]

DapEs hydrolyze N-succinyl-L,L-diaminopimelic acid (L,L-SDAP) to L,L-diaminopimelic acid (L,L-DAP) and succinate (Figure 1). All DapE enzymes characterized to date are members of the M20 family of dinuclear Zn(II)-dependent metalloproteases and exist as dimers comprised of a catalytic domain, an eight-stranded twisted β-sheet that is sandwiched between seven α-helices that contains the catalytic active site, and a thioredoxin-like dimerization domain.[11] The active site is comprised of strictly conserved residues located on five loops, containing either one or two zinc ions, and is exposed to the solvent.[10] In general, the other members of the M20 family are either monomeric or homo-dimeric and appear to have very similar tertiary structures with retention of nearly identical active site Zn(II) ligands. Of particular interest are the structural features employed by DapE enzymes to hydrolyze L,L-SDAP, particularly around substrate selectivity,[12] with the ultimate goal of designing inhibitors as potential antibiotics.

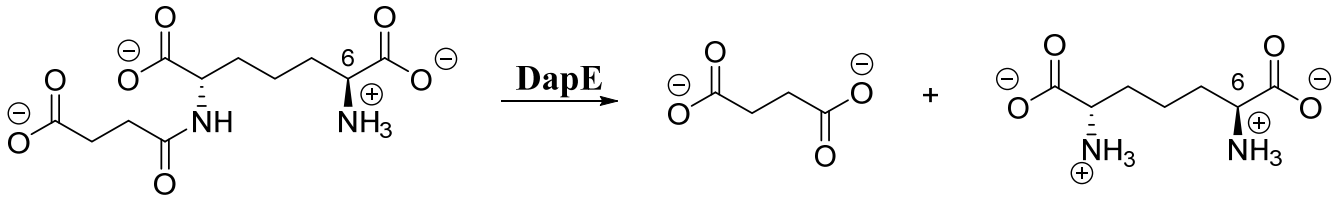

Figure 1. Enzymatic cleavage of LL-SDAP (**1**) by DapE yielding succinate (**2**) and LL-DAP (**3**)

To elucidate the structural features critical for DapE enzymes to recognize and bind L,L-SDAP and the catalytic mechanism of its hydrolysis, we have determined the X-ray crystal structure of [ZnZn(*Hi*DapE)] bound by the products of hydrolysis, succinic acid and L,L-DAP.

The products-bound structure of [ZnZn(*Hi*DapE)] reveals previously unknown substrate-enzyme interactions and a catalytically significant, dramatic conformational change, that positions residues from the B subunit in the active site of the A subunit. In addition, the newly formed amine of L,L-DAP is only 2.9 Å from the newly formed succinic acid carbon allowing the use of a new protocol that we refer to as product-based transition-state modeling (PBTSM)[13] to model possible catalytic intermediates. The combination of these data provides new insight into substrate recognition and binding as well as the catalytic mechanism of DapE enzymes.[5,10]

EXPERIMENTAL PROCEDURES

Materials. D,L-α,ε-Diaminopimelic acid (98%), succinic anhydride and ion exchange resin (Dowex 50WX8 − 200,H^+ form) were purchased from Sigma. 2-Naphthalenesulfonic acid 1-hydrate (98%) was purchased from TCI and Microcrystalline cellulose was purchased from Merck. All other chemicals were purchased from commercial sources and were of the highest quality available.

Protein Expression and Purification. Cloning, expression and purification of DapE enzymes were performed according to the standard protocol as described previously for *Hi*DapE[11] and the dapE from *Neisseria meningitidis* (*Nm*DapE).[14] The cell pellet was thawed and sonication was used to disrupte the cells. The cell debris was pelleted by centrifugation at 15,000 rpm for 40 min. at 4 °C. The supernatant was loaded onto a column packed with 10 mL of HisTrap HP resin (GE Healthcare), and washed with 20 bed volumes of lysis buffer. The His_6-tagged *Hi*DapE enzyme was eluted with 25 mL of elution buffer (500 mM NaCl, 5% glycerol, 50 mM HEPES, pH 8.0, 250 mM imidazole, 10 mM 2-mercaptoethanol). The His_6-tag

was removed by treating His_6-tagged *Hi*DapE with His_6-tagged TEV protease for 16 h at 4 ˚C in 50 mM HEPES, pH 8.0. Cleaved protein was concentrated with a Centricon (30.000-MW cutoff; Amicon) to 3 mL and loaded on a HiLoad 16/600 Superdex 200 Prep Grade column (GE Healthcare) for further purification. The resulting solution was mixed with 5 mL of His-Trap HP resin packed on a column to remove the remaining cleaved His_6-tag, uncut protein and the His_6-tagged TEV protease, while the flow through containing *Hi*DapE was collected and washed with crystallization buffer (150 mM NaCl, 20 mM HEPES pH 8.0, and 1 mM TCEP) and concentrated to ~20 mg/ml.

Site Directed Mutagenesis. In the manner as previously described,[11] the *Nm*DapE site-directed mutant H195A (corresponding to H194 in *Hi*DapE) was introduced on a plasmid carring WT *Nm*DapE using a modified PIPE cloning procedure PMID:21185308. Briefly, the following primers were used to amplify the dapE gene encoding for *Nm*DapE, H195A-F; CAA GCA AGG CGC TAT TGC CTA TCC GCA TTT GGC AAT CAA TC, *Nm*DapE, H195A-R; TAG GCA ATA GCG CCT TGC TTG CCT TTG ACG GTC A. The unpurified product of amplification was treated with T4 polymerase and transformed to chemically competent BL21-Gold (DE3) cells. The presence of both mutations was confirmed by sequencing at University of Chicago Cancer Research DNA Sequencing Facility. Purification of *Nm*DapE H195A mutant enzyme was conducted as described above for *Hi*DapE.

Enzymatic Assay. SDAP was synthesized using the procedure described by Lin *et al*.[15] providing an overall yield of 41%. The specific activity of all *Hi*DapE and *Nm*DapE proteins were determined using a 50/50 mixture of D,D and L,L-SDAP as the substrate in 50 mM Phosphate buffer (PPi) or 50 mM HEPES, pH 7.5 as previously described.[12] The kinetic parameters V_{max} and K_m were determined by quantifying amide bond cleavage (decrease in

absorbance) of L,L-SDAP at 225 nm ($\varepsilon = 698\ M^{-1}\ cm^{-1}$) in triplicate using a Shimadzu UV-2450 spectrophotometer equipped with a temperature controller. Enzyme activities are expressed as units/mg where one unit is defined as the amount of enzyme that releases 1 μmol of L,L-SDAP at 30 ˚C in 1 min. Catalytic activities were determined with an error of ± 10 %. Initial rates were fit directly to the Michaelis-Menten equation to obtain the catalytic constants K_m and k_{cat} using Origin software.

Crystallization. Prior to crystallization, 50 mM L,L-SDAP was added to *Hi*DapE and equilibrated on ice for 30 min. Almost three hundred commercially available conditions were used for screening by the sitting-drop vapor-diffusion method at 16 °C using a Mosquito liquid handling robot with 96 well plates. Crystals were observed in 10 different conditions within three weeks. The best crystals were obtained using 400 nL of a precipitant solution (0.05 M HEPES pH 7.3, 10.7% (w/v) PEG MME 2000, and 8.6 % (w/v) PEG 2000) and 400 nL of 18 mg/mL solution of *Hi*DapE. The crystals belonged to the orthorhombic space group I222 with unit cell parameters a =56.6 Å, b = 135.5 Å, c = 149.6 Å, and α = β = γ = 90°, with one molecule in the asymmetric unit (Table 1). *Hi*DapE is a dimer and the protein two-fold axis coincides with the crystallographic axis. Prior to data collection the mother liquid, containing 25% glycerol, was used as a cryoprotectant. The crystal was retrieved with a nylon loop (Molecular Dimensions) and flash-frozen in liquid nitrogen.

Structure Determination. The presence of Zn ions in the protein crystals of *Hi*DapE was confirmed by X-ray fluorescence spectroscopy. Data were collected on the 19-ID beamline of the Structural Biology Center at the Advanced Photon Source using SBC-Collect software at a wavelength of 0.9795 Å from the single crystal and the data were processed using HKL3000.[16] Crystallographic parameters are summarized in Table 1. The structure of the complex of

*Hi*DapE was determined by molecular replacement using the catalytic and dimerization domains separately (PDB ID 4H2K and 3ISZ, respectively) as search models.[10,11] Molecular replacement searches were completed using MOLREP of the CCP4 suite.[17] The initial model was adjusted manually and refined using programs REFMAC XX[18] and Phenix.[19] The final models were refined against all reflections except for 5% randomly selected reflections, which were used for monitoring R_{free}. The final rounds of refinement were carried out using TLS refinement with three TLS groups, and the final refinement statistics are presented in Table 1. Analysis and validation of the structures were performed with the aid of MOLPROBITY and COOT validation tools.[20,21] Figures were prepared using Pymol and the Chemical Computing Group's Molecular Operating Environment (MOE).[22]

Protein Data Bank accession code. The atomic coordinates and structure factor file for the [ZnZn(*Hi*DapE)] product-bound structure have been deposited in the RCSB Protein Bank with accession code 5VO3.

Chemical Modification Reagents. The arginine-specific chemical modification reagent, 2,3-butanedione was tested as an inhibitor of *Hi*DapE. A 1.0 M 2,3-butanedione solution was prepared in 50 mM borate buffer, pH 7.8 and added to 1 μM *Hi*DapE in the dark in 50 mM borate buffer, pH 7.8, to provide final 2,3-butanedione concentrations of 0, 10, 20, 40, and 80 mM. Since it is possible for 2,3-butanedione to act as a photosensitizing agent and cause the modification of other residues, the experiments were done in triplicate in the dark to verify that the loss in DapE activity was the result of the modification of arginine residues. Similarly, the lysine specific reagent, 2,4,6-trinitrobenzene sulfonate was also shown to inhibit the hydrolysis of L,L-SDAP by *Hi*DapE in 50 mM phosphate buffer, pH 7.8, at 25 ºC. The concentrations of 2,4,6-trinitrobenzene sulfonate used were 0, 2.5, 10 and 20 mM.

In-Silico Modeling. Product-based transition-state modeling (PBTSM)[13] was performed using the Chemical Computing Group's Molecular Operating Environment (MOE).[22] The *Hi*DapE product-bound crystal structure (PDB ID: 5VO3) was used as the starting point for PBTSM. The crystallographic data were prepared using MOE's utility structure-prep to correct for any artifacts.[22] The model was then solvated in a simple box of water at pH of 7.4 that contained NaCl counter ions for charge balance. Periodic boundary conditions were enabled and the hydrogen bonding network of the model was optimized by sampling different tautomer/protomer states using Protonate3D.[23] A localized energy minimization was run on the solvated system using the MOE function QuickPrep, followed by a short global minimization to equilibrate the system. Product atom coordinates were used to model the tetrahedral transition-state and the subsequent substrate-catalytic hydroxyl bound structure, and the substrate binding step. In each case, the hydrogen bonding network and formal charges were optimized so the overall net charge of the system remained balanced. A localized minimization was conducted for each intermediate to normalize the bond distances and angles followed by a 1.0 ns molecular dynamics (MD) equilibration using an NPA algorithm with an Amber12:EHT force-field. MD experiments utilized an initial heating from 0 K to 300 K over 100 ps followed by equilibration for 100 ps at 300 K, after which a 700 ps production run was performed. Finally, a 100 ps cooling from 300 K to 0 K was carried out.

Results and Discussion

Conformational change upon substrate binding. DapE enzymes have strict specificity for the L,L-isoform of SDAP and this specificity is built into the active site, which includes both the

dinuclear metal cluster as well as adjacent amino acid residues.[24] A well-defined and negatively charged, crescent-shaped cavity was previously identified in the [ZnZn(*Hi*DapE)] structure.[5,10] Considering the linear character of the substrate, it was hypothesized that the substrate binds in this crescent-shaped cavity lining up along the grove with the peptide bond positioned over the active site metal ions; however, the exact binding conformation of L,L-SDAP is unknown. In the WT [ZnZn(*Hi*DapE)] structure, the catalytic and dimerization domains adopt an extended conformation with dimensions 50×44×121 Å with the crescent-shaped cavity located between the two domains. The center of the catalytic domain that coordinates the metal ions is broadly open, allowing substrate access to the dinuclear Zn(II) active site (Figure 2A).[10] Substrate poses developed by docking L,L-SDAP along this grove positioned the substrate carbonyl carbon near Zn1.

The addition of L,L-SDAP to [ZnZn(*Hi*DapE)], prior to crystallization, yielded orthorhombic crystals found to exhibit a different space group (I222) from that of wild-type [ZnZn(*Hi*DapE)] ($P2_12_12_1$), which diffracted to 1.95 Å. The structure that emerged revealed [ZnZn(*Hi*DapE)] bound by the products of hydrolysis, succinic acid and L,L-DAP, which are clearly observed in the 2*Fo-Fc* omit maps (Figure 3A). Surprisingly, the products-bound structure revealed that the *Hi*DapE enzyme had undergone a significant conformational change that shrinks the enzyme in size with overall dimensions of 47×45×111 Å (Figure 2B). Overlay of the open WT [ZnZn(*Hi*DapE)] structure with the closed [ZnZn(*Hi*DapE)] products-bound structure reveals that in the products-bound-conformation, the catalytic domain rotates ~50 degrees and shifts as much as 29 Å at the exterior of the protein and 10 Å at the protein center of the catalytic domains (as measured at the position of the Zn atoms) (Figure 2C & 2D). This heretofore unobserved closed conformation revealed significant movements within the catalytic

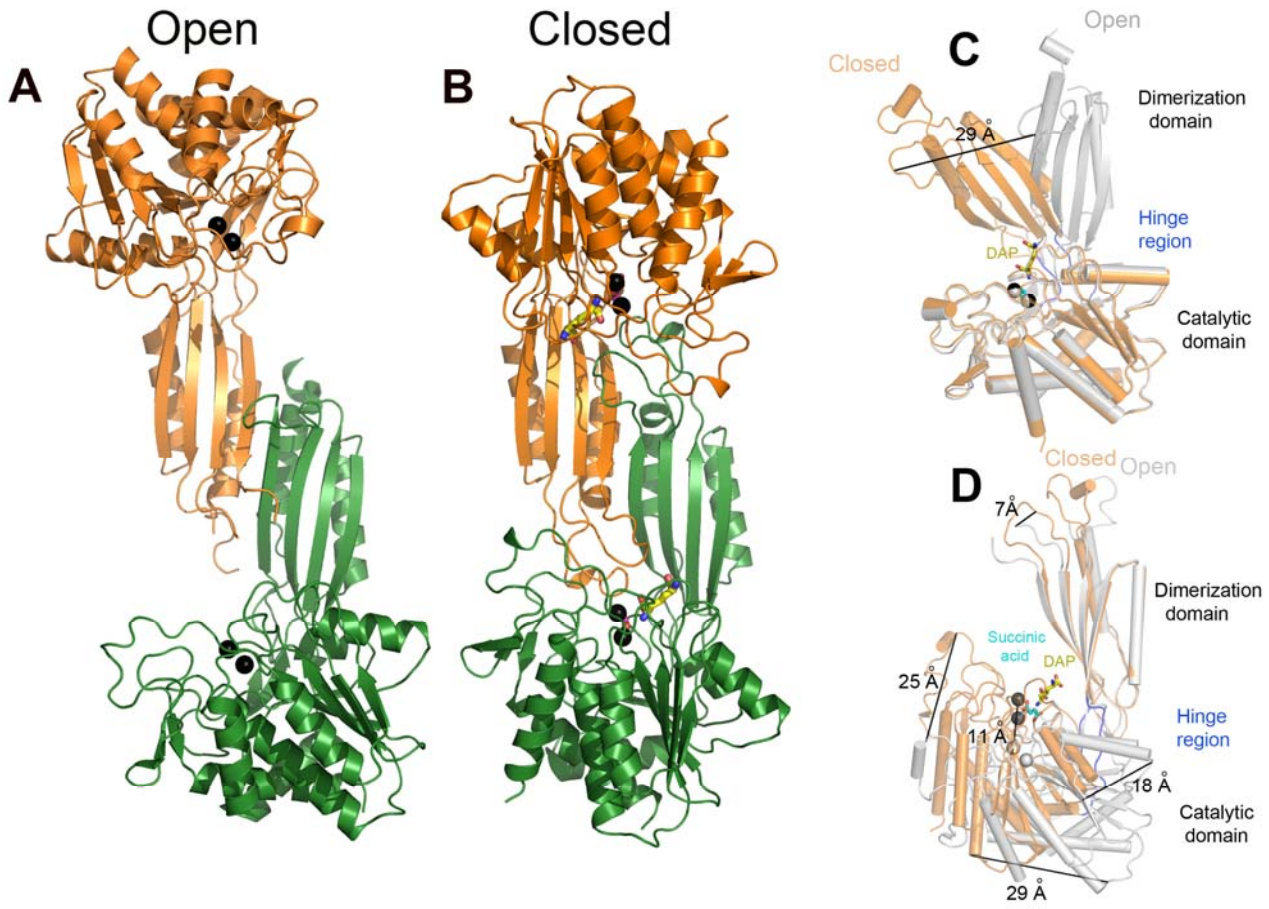

Figure 2. Side-by-side comparison of structures of *Hi*DapE in two different conformations. **A**) Ribbon diagram of previously reported holoenzyme structure of *Hi*DapE in its "open" conformation (PDB 3IC1). **B**) Structure of the complex of *Hi*DapE with the products succinic acid (in magenta) and L-diaminopimelic acid (in yellow), in the closed conformation. Individual subunits of the homodimer are colored green and orange. Panels **C** and **D** show the complexity of the domain movements for *Hi*DapE. **C**) Shows the extent of rotational conformational changes as observed by superimposition of the catalytic domains of the monomers of open (gray) and closed (orange) structures, while **D**) shows the movement within the dimerization and catalytic domains as revealed by superimposition of the dimerization domains of the open and the closed conformation structures.

domain compared to [ZnZn(*Hi*DapE)], which results in effectively closing off access to the dinuclear Zn(II) active site (Figure S1). Moreover, several new protein-ligand interactions, that had not previously been observed or predicted by either docking attempts or molecular dynamics studies conducted on the open, WT [ZnZn(*Hi*DapE)] structure, are revealed. These data also disclose the surprisingly flexible nature of the DapE active site.[25]

The closed [ZnZn(*Hi*DapE)] products-bound structure illustrates that the substrate binding pocket can be divided into succinic acid and L,L-DAP binding regions (Figure 3A), with the succinic acid binding pocket positioned adjacent to the dinuclear Zn(II) active site, as highlighted by the cyan box in Figure 3B. The succinate carboxylate group bound to the dinuclear Zn(II) cluster exhibits Zn-O atom bond distances of: Zn1-O1 1.9 Å, Zn2-O1 2.5 Å, Zn1-O2 4.1 Å, and Zn2-O2 2.1 Å. The Zn2-O1 bond distance of 2.5 A is too long for a covalent bonding interaction, as the average Zn-O(carboxylate) bond distance in proteins is 2.01 Å and is at the limit of their van der Waals radi.[26] Therefore, the succinate carboxylate moiety bridges the dinculear Zn(II) cluster in a μ-1,3 fashion forming a bis(μ-carboxylato)dizinc(II) core with a Zn-Zn distance of 3.8 Å (Figures 3A & 5A). Both Zn(II) ions reside in distorted tetrahedral or trigonal bipyramidal (TBP) geometries with the oxygen atom of Asp100 (2.0 Å) and the dangling oxygen atom of Glu163 (2.6 Å) making up the axial positions of a potential TBP geometry for Zn1 while the oxygen atom of Asp100 (1.9 Å) and the dangling oxygen atom of Glu135.A (2.4 Å) making up the axial positions of a potential TBP geometry for Zn2.

The other carboxylate group of the succinic acid moiety forms a salt bridge with the ammonium groups of Arg178.A (2.9 and 3.1 Å) and an H-bonding interaction between the O1 atom and aromatic hydroxyl hydrogen of Tyr197.B (2.4 Å), from the opposing dimerization domain. Moreover, a water molecule is observed bridging the O2 atom of succinic acid (2.8 Å)

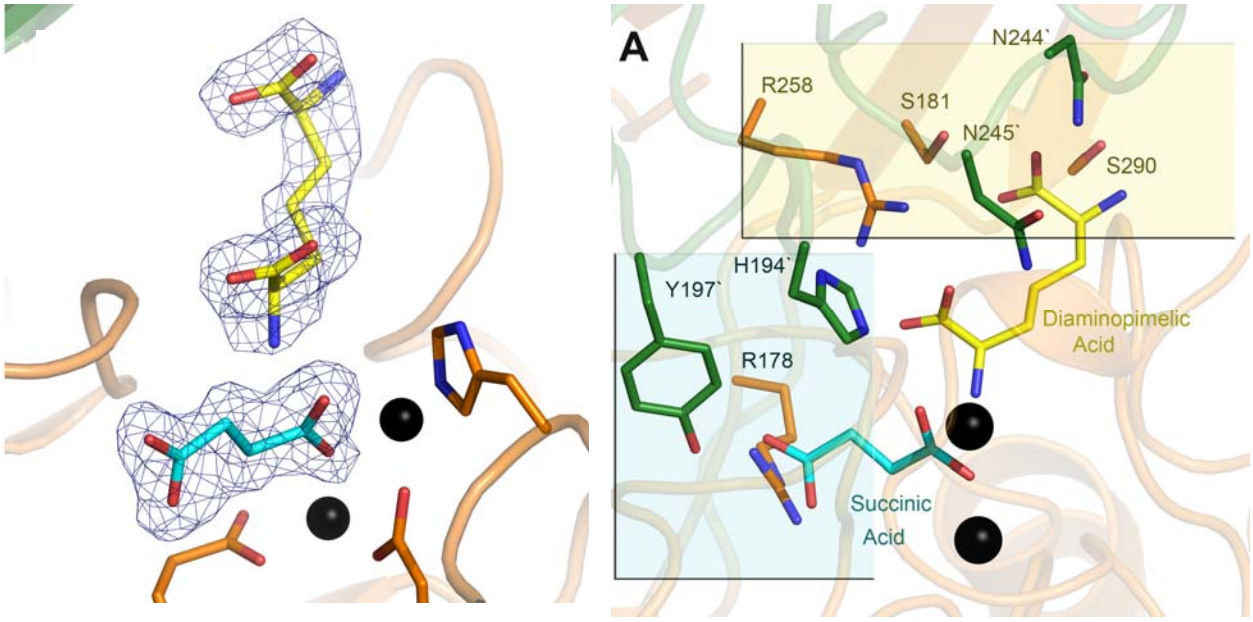

Figure 3. Close-up view of *Hi*DapE bound by the products of LL-SDAP hydrolysis: succinic acid (cyan) and L-diaminopimelic acid (in yellow), and the interacting side chains and zinc ions. **A**) $F_o - F_c$ omit map of the products at 3.5 σ. **B**) The side chains are colored orange or green to highlight the contribution of residues in both subunits of the homodimer. Residues interacting with succinic acid or LL-DAP are highlighted in cyan and yellow boxes, respectively.

and the N atom of the ammonium group of Lys175.A (3.0 Å). Given this interaction, we examined the ability of the Lys-specific reagent, 2,4,6-trinitrobenzene sulfonate, which forms a stable covalent complex with free amines, to inhibit [ZnZn(*Hi*DapE)]. Upon incubation of [ZnZn(*Hi*DapE)] with 2,4,6-trinitrobenzene sulfonate, the enzyme quickly loses catalytic activity both in a time- and a 2,4,6-trinitrobenzene sulfonate concentration-dependent fashion (Figure S2B). These data suggest that at least one Lys residue is involved in substrate binding, consistent with the [ZnZn(*Hi*DapE)] products-bound structure. The observed [ZnZn(*Hi*DapE)]

interactions with succinic acid echo some of the interactions observed in the DapE-captopril inhibitor complex.[14]

L,L-DAP, on the other hand, does not bind to the dinuclear center, but interacts solely through contacts between its carboxylate groups with the enzyme side chains Asn244.B, Asn245.B, Ser181.A, Ser290.A, and Arg258.A as shown in the yellow box in Figure 3B. It is noteworthy that nearly all of these residues are strictly conserved in DapE enzymes.[24] Additional evidence that an Arg residue interacts with substrate was obtained with the arginine-specific chemical modification reagent, 2,3-butanedione. Upon the addition of 2,3-butanedione to [ZnZn(*Hi*DapE)], catalytic activity is lost in a time and inhibitor concentration-dependent fashion indicating that at least one arginine residue interacts with the substrate (Figure S2A). As confirmed by the [ZnZn(*Hi*DapE)] products-bound structure, the terminal L,L-DAP carboxyl group forms hydrogen bonding interactions with one arginine residue, Arg258.A, which is located near the hinge region of DapE. Consequently, this hydrogen bonding interation, along with those for Asn244.B and Asn245.B, likely drive the open *Hi*DapE conformation to close in combination with Coulombic interactions *via* the succinic acid portion of the substrate with Tyr197.B and His194.B. Therefore, binding of the substrate induces the dimer superstructure to flex and twist at the hinge region resulting in dynamic modulation during catalysis. Initially, this dynamic modulation occurs to accommodate the substrate in the active site and then to position active site residues, including those from the dimerization domain of the opposite chain, for catalytic turnover. The overall characteristic of this closure movement is consistent with a hinge domain movement mechanism,[27-29] that allows a twist and turn movement of the inter-domain linker.

Surprisingly, His194.B, which is located on the dimerization domain of the opposing

chain ~10.1 Å away from the dinuclear Zn(II) active site in the WT structure (Figure 4A), forms a hydrogen bond (2.9 Å) with the oxygen atom of succinic acid bound to Zn2 in the [ZnZn(*Hi*DapE)] products-bound structure (Figure 4B). This results in the formation of an oxyanion hole made up of Zn(II) and His194.B that forms in the closed structure. As the closed structure forms upon substrate binding, the movement of His194.B more than 10 Å is critical as it assists in activating the scissile carbonyl carbon of the substrate for nucleophilic attack by a hydroxide nucleophile and also helps to stabilize the transition-state. The concept of an oxyanion hole is a well-established enzyme characteristic in biochemistry, specifically when referring to serine or serine-like hydrolase/peptidase enzymatic functions.[30,31] As *Hi*DapE exhibits >60% of its maximal activity when only one Zn(II) ion is present on the Zn1 side of the dinuclear active site, His194.B likely plays a crucial role in activating the carbonyl carbon of L,L-SDAP in the absence of Zn2, possibly forming an oxyanion hole with the Zn2 ligand His349.A. Sequence alignment with multiple DapE's[32] (Figure S3) confirms that H194 in *Hi*DapE is highly conserved. Mutation of His195.B in *Nm*DapE,[14] which corresponds to H194.B in *Hi*DapE, provides a [ZnZn(*Nm*DapE)] enzyme that exhibits only ~3% of its WT activity. These data indicate that H194.B is critical for catalytic activity in the presence of two Zn(II) ions, but is not essential. Therefore, the [ZnZn(*Hi*DapE)] products-bound structure demonstrates that residues residing in both domains play key roles in catalysis and significantly, residue His194.B of *Hi*DapE, had not previously been identified as a catalytically important residue.

Modeling the DapE catalytic reaction. Our recently-reported product-based transition-state modeling (PBTSM) method[13] was employed, using the [ZnZn(*Hi*DapE)] product-bound structure as a starting point structure (Figures 5A & 5B).[13] PBTSM is a reverse engineering approach that provides catalytic models for the lowest energy structures of each major

A

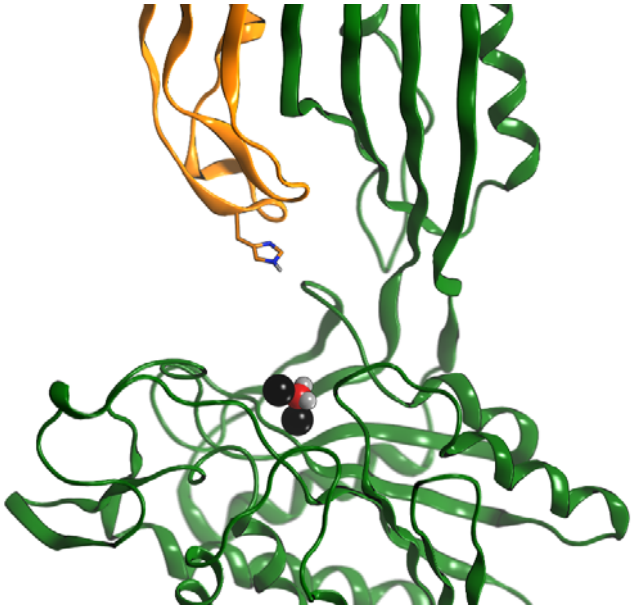

B

Figure 4. (**A**) *Hi*DapE open conformation showing the distal location of H194.B (**B**) Proposed oxyanion hole formed by H194.B and Zn2 in the catalytically-active closed form of *Hi*DapE.

catalytic step, using a combination of molecular mechanics and molecular dynamics in reverse chronological order. This modeling technique was performed using the Chemical Computing Group's Molecular Operating Environment modeling suite (MOE).[22] The [ZnZn(*Hi*DapE)] product-bound structure atom coordinates were used to model the tetrahedral transition-state complex, which reflects the moment immediately after nucleophilic attack by a hydroxyl group at the amide carbonyl carbon of the substrate (Figures 6A & 6B). In the [ZnZn(*Hi*DapE)] product-bound structure, the scissile carbonyl carbon is 2.9 Å away from the ammonium

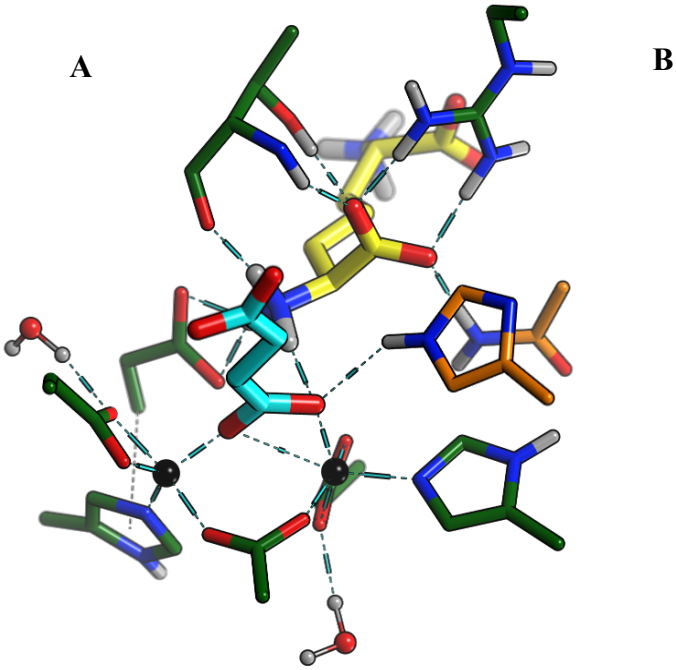

Figure 5. **A**) Radial and **B**) Axial view of *Hi*DapE's binding pocket with succinate acid and LL-DAP bound in the closed conformation, generated from crystal structure PDB ID #### utilizing the PBTSM protocol. Atomic color scheme associated with succinate and LL-DAP shown in cyan and yellow while protein chains A and B are shown in dark green and orange, respectively. The Zn(II) ions are shown as black spheres, waters as red, and amino groups as dark blue and red for nitrogen and oxygen, respectively.

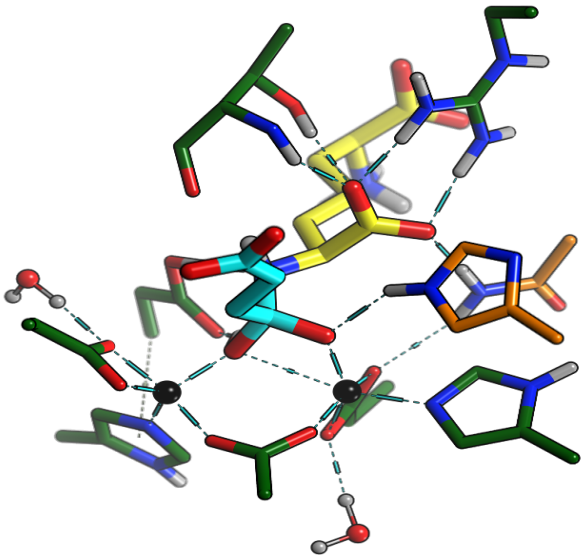

Figure 6. PBTSM generated models showing the **A**) Radial and **B**) Axial view of *Hi*DapE's bindng pocket with the LL-SDAP transition-state complex bound in the closed conformation. Color scheme is identical to that in Figure 5.

nitrogen of L,L-DAP (Figure 5B), allowing for the reformation of an amide bond using the Builder utility in MOE, creating a distorted tetrahedral intermediate complex. Application of the correct formal charges for the ammonium nitrogen and the alkoxide oxygen associated with the amide carbonyl of the substrate, was followed by hydrogen bond network optimization. These critical system adjustments notably affected the ionization states and hydrogen bonding interactions of Glu134.A, which was previously shown to function as the general acid-base.[24] A local minimization was conducted to normalize the bond distances and angles of the L,L-SDAP-OH tetrahedral intermediate as well as balance the net charges of the ligand/receptor system after

which a 1.0 ns molecular dynamics equilibration was performed using an NPA algorithm with an Amber12:EHT force field.[33,34]

The model developed for the tetrahedral intermediate based on the [ZnZn(HiDapE)] products-bound structure reveals several interesting aspects of the catalytic mechanism (Figures 6A and 6B). First, an increase in the Zn-Zn distance from 3.8 to 4.0 Å was observed along with improvement in the hydrogen bond network. Since *Hi*DapE exhibits >60% of its maximal activity when a single Zn(II) ion bound in the Zn1 side of the dinuclear active site,[10] the O1 atom of the modeled transition-state complex bound to Zn1 represents the hydroxide oxygen atom while the O2 atom bound to Zn2 is due to the substrate carbonyl carbon (Figure 6A). The increase in Zn-Zn distance also increases the O1-Zn2 distance to >2.6 Å, which reinforces the proposal that the nucleophilic hydroxide is bound to and delivered by Zn1. The combination of His194.B retaining a strong hydrogen bonding interaction with O2 along with coordination of O2 to Zn2 is consistent with this being an alkoxide moiety derived from the substrate carbonyl group. This model also reveals that Glu134.A forms hydrogen bonds to both the succinc acid O1 oxygen atom as well as the L,L-DAP amide nitrogen atom, consistent with its proposed role as a general acid/base.[24]

Interestingly, a single oxygen atom bridge does not exist between the two-active site Zn(II) ions. This finding is in contrast to Zn K-edge EXAFS spectra of [ZnZn(*Hi*DapE)] in the presence of the competitive, transition-state analog inhibitor 2-carboxyethylphosphonic acid (CEPA), which indicated that the Zn−Zn distance remained unchanged at 3.34 Å.[35] The fact that the Zn−Zn distance does not change upon CEPA binding to [ZnZn(*Hi*DapE)] suggests an η-1-μ-phosphonate bridge exists, similar to the binding mode of leucine phosphonic acid to the leucine aminopeptidase from bovine lens.[36] As this is clearly not the case for the actual substrate

transition-state complex for [ZnZn(HiDapE)] based on the PBTSM transition-state model and the [ZnZn(HiDapE)] products-bound structure, the difference is likely due to the heretofore previously unknown open and closed conformations of DapE. CEPA would not interact with the residues located near the hinge region of DapE, such as Asn244.B and Arg258.A, which likely drive the formation of the closed structure and clearly form hydrogen bonding interations with the substrate functional groups in the tetrahedral (transition-state) complex (Figure 6B) and the [ZnZn(HiDapE)] products-bound structure (Figure 5B). These data emphasize the importance of the newly discovered closed structure and its impact not only on the catalytic reaction mechanism, but also on the future design of new, potent inhibitors of DapE enzymes.

Using the transition-state model derived from the [ZnZn(*Hi*DapE)] products-bound structure, the atomic coordinates for the catalytic hydroxyl group and native substrate bound to [ZnZn(HiDapE)] were calculated. This model reflects the moment just after deprotonation of the catalytic water by the general acid-base, Glu134.A, but just before nucleophilic attack by the activated hydroxyl group at the substrate amide carbonyl. MOE's Builder utility was utilized to remove the bond between the tetrahedral carbonyl carbon and the O1 oxygen atom, the oxygen bound to Zn1. An ionization state adjustment of the newly formed catalytic water/hydroxide oxygen to a negative (O^--C---X---OH to O^--C $^-$OH) is also required. Thus, the catalytic hydroxyl group, coordinated to Zn1, was modeled into the system in the approximate area observed in other known crystal structures of DapE.[10,11,14] Next, a double bond was created, reforming the substrate carbonyl moiety (O^--C-NH to O=C-NH). As with the tetrahedral intermediate model, a local minimization was initiated to correct bond angles and distances after which a 1.0 ns molecular dynamics equilibration was performed (Figure 7A & 7B). This model reveals that the nucleophilic hydroxide is located on Zn1 while the substrate carbonyl oxygen

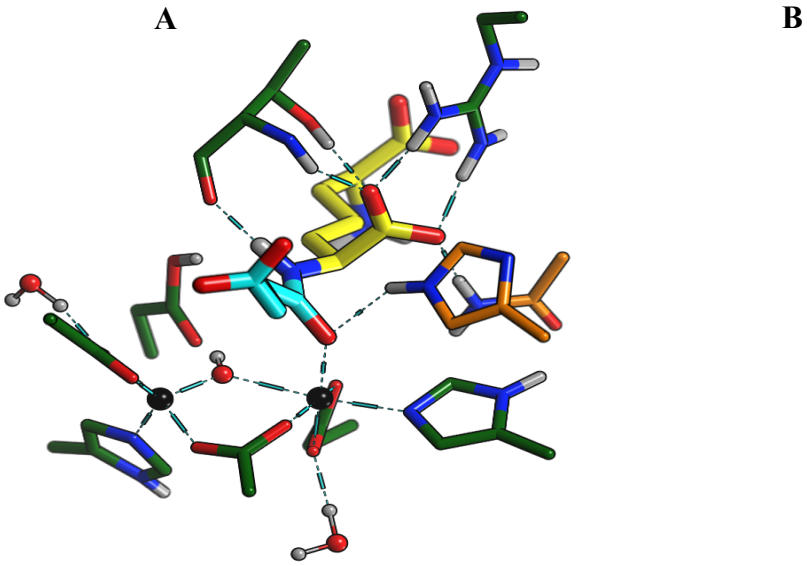

Figure 7. PBTSM generated models showing the **A**) Radial and **B**) Axial view of *Hi*DapE's bindng pocket with LL-SDAP and the activated catalytic hydroxyl group bound in the closed conformation. Color scheme is identical to Figure 5.

atom is coordinated to Zn2 with His194.B forming a hydrogen bond to the O2 carbonyl oxygen atom. This oxyanion hole activates the sissile carbonyl carbon for nucleophilic attack. The closed, crescent-shaped substrate binding pocket positions the sissile carbonyl carbon above the hydroxide moiety bound to Zn1 (2.9 Å), preorganizing the substrate for nucleophilic attack. This model clearly shows the role of both Zn(II) ions in catalysis and reinforces the importance of substrate hydrogen bonding interactions with Arg, Asn, and Lys residues in subunit A and near the hinge region of subunit B.

Finally, PBTSM was applied to the catalytic hydroxyl group and native substrate bound [ZnZn(*Hi*DapE)] model to estimate the atomic coordinates of the initial substrate binding step to [ZnZn(*Hi*DapE)]. This model reflects the moment just after substrate binding and the

displacement of the bridging water molecule observed in the WT [ZnZn(*Hi*DapE)] structure and subsequent conformational closure of the active site. This model's point in time also falls just before deprotonation of the catalytic water by Glu134.A. The model was generated by deprotonating Glu134.A along with the simultaneous protonation of the catalytic hydroxyl group and the formation of an O1-Zn2 bonding interaction. Protonate3D was used followed by QuickPrep to reoptimize the hydrogen bonding network. A localized energy minimization step was then applied to the system followed by a 1.0 ns molecular dynamics equilibration (Figure 8A & 8B). This model contains a (μ-aquo)(μ-carboxylato)dizinc(II) core with a Zn-Zn distance of 3.4 Å with one terminal carboxylate and one histidine residue at each metal site (Figure 8A). The amide carbonyl of L,L-SDAP is positioned near Zn2 while the amide N-H acts as an hydrogen bond donor to the backbone carbonyl of Thr325.A, a residue that was previously

A **B**

Figure 8. PBTSM generated models showing the **A**) Radial and **B**) Axial view of *Hi*DapE's bindng pocket with LL-SDAP and the unactivated catalytic water bound in the closed conformation. Color scheme is identical to Figure 5.

implicated as catalytically important.[37] In addition, His194.B moves into the active site and forms an oxyanion hole along with Zn2, via a strong hydrogen bonding interaction with the amide carbonyl oxygen, O2. The proximal carboxylate of L,L-SDAP participates in bifurcated hydrogen bonds with the side chains Arg258.A, Thr325.A and Asn245.B (Figure 8B). The free primary amino group acts as an hydrogen bond donor to the backbone carbonyl of Ala136.A and a water molecule, which in turn participates in hydrogen bond donation to the backbone carbonyl of Glu135.A and the side chain carbonyl of Asn245.B. The terminal carboxylate of the pimelic acid moiety is hydrogen bonded to the N-H of Asn244.B, the side chain hydroxyl of Ser181.A and Ser290.A, and a water molecule, which in turn forms an H-bond to the side chain hydroxyls of Thr183.A and Thr325:A.

Implications for the Catalytic Mechanism of DapE. The [ZnZn(*Hi*DapE)] product-bound structure and modeling studies described herein enables further refinement of the previously proposed catalytic mechanism for DapE enzymes to include the important catalytic roles played by dimerization domain residues in recognition and binding of the substrate and activation of the amide carbonyl (Figure 9).[5] Combination of the data presented herein along with all the available DapE structures and the previously reported kinetic and spectroscopic data,[38] suggests that the first step in catalysis for DapEs is the recognition of L,L-SDAP by the crescent-shaped cavity adjacent to the dinuclear Zn(II) cluster with the enzyme in the open conformation. Substrate binding induces a conformational change, resulting in the closed DapE structure, that positions the amide carbonyl oxygen, O2, of L,L-SDAP adjacent to Zn2 and triggers the formation of an oxyanion hole by shifting His194.B from the dimerization domain of the B protein strand into the active site. Formation of a strong hydrogen bond between His194.B and the amide carbonyl oxygen atom facilitates coordination to Zn2, thus displacing the bridging

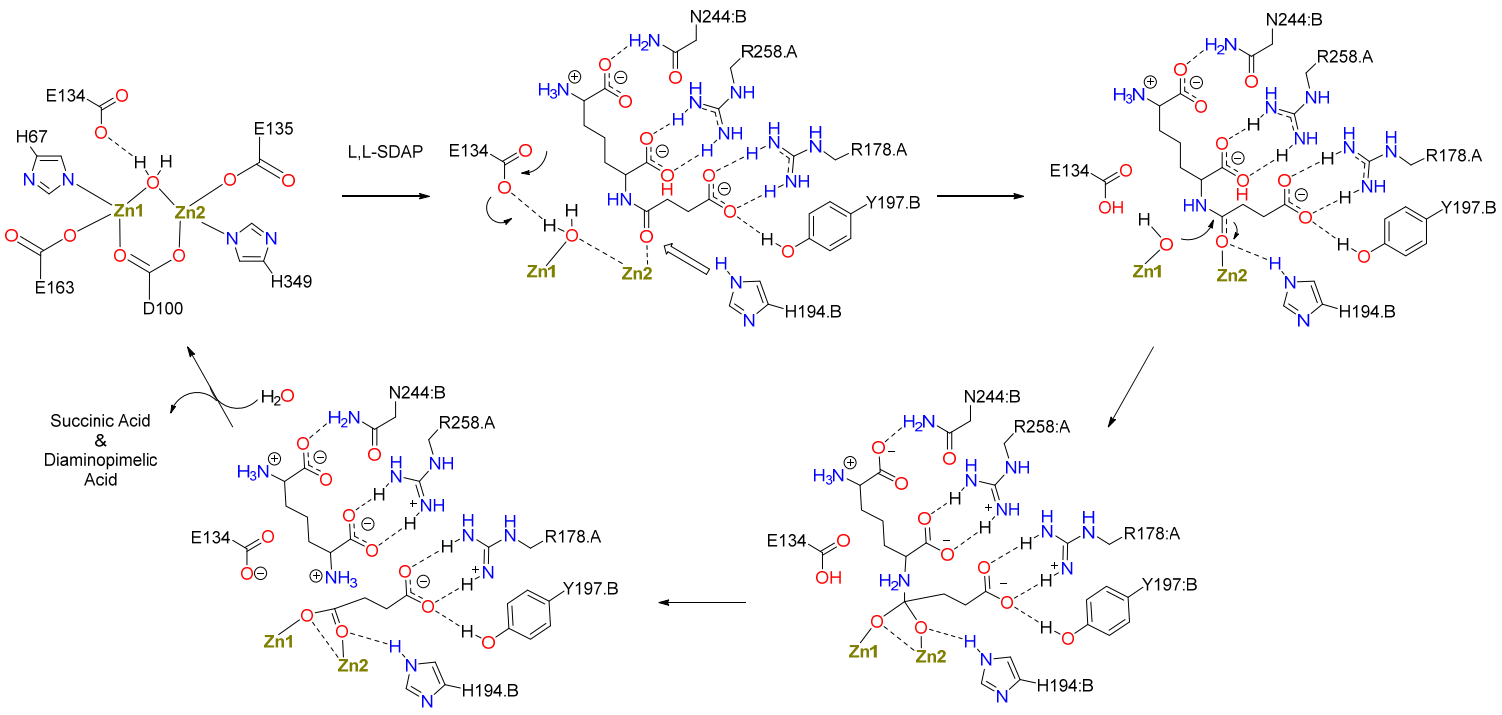

Figure 9. Proposed catalytic mechanism for the hydrolysis of LL-SDAP by DapE enzymes.

water molecule onto Zn1 and activating the sissile carbonyl carbon for nucleophilic attack. Deprotonation of the Zn1-bound water molecule by Glu134.A forms a nucleophilic hydroxide moiety, consistent with the postulated pK_a of the Zn(II)-bound water molecule.[24] Once the Zn1-bound hydroxide is formed, it can attack the activated carbonyl carbon of the substrate, forming an η-1,3-μ-tetrahedral transition-state complex. Solvent kinetic isotope effect studies yielded an inverse isotope effect that was explained by the attack of a Zn(II)-bound hydroxide on the amide carbonyl.[24] As observed for similar M20 metalloenzymes, such as the aminopeptidase from *Aeromonas proterlytica* (AAP) and further confirmed by the [ZnZn(*Hi*DapE)] product-bound structure, Glu134.A provides a proton to the penultimate amino nitrogen returning it to its ionized state. Upon cleavage of the amide bond, the tethering interaction of the products that maintains the closed enzyme conformation is disrupted. Release of the products is entropy

driven, facilitating reformation of the open DapE conformation with the addition of a bridging water molecule.

In the absence of Zn2, the catalytic mechanism is not expected to markedly change as substrate binding will still likely induce the formation of the closed conformation moving His194.B into the active stite, likely forming an oxyanion hole with the Zn2 ligand His349.A. This oxyanion hole would activate the amide carbonyl allowing for nucleophilic attack by the Zn1-bound hydroxide. The remaining steps in the mechanism would be the same as that proposed for the dinuclear Zn(II) enzyme except that His349.A and His194.B would function to stabilize of the tetrahedral transion-state, analagous to that proposed for the mono-metallated forms of AAP and the methionine aminopeptidase from *E. coli*.[39-41]

Acknowledgements

The authors (CR; AS; TH) wish to thank members at the MCSG and CSGID centers located in Argonne National Laboratory for training in state-of-the-art high-throughput technologies and methodologies to purify and characterize the three dimensional protein structures. This work was supported by the National Institute of Health (NIH) and the National Institute of Allergy and Infectious Diseases (NIAID) [contracts HHSN272200700058C and HHSN272201200026C to the Center of Structural Genomics of Infectious Diseases], the National Science Foundation (CHE-1412443, RCH) and the Todd Wehr Foundation (RCH). The use of Structural Biology Center beamlines at the Advanced Photon Source was supported in part by the U.S. Department of Energy, Office of Biological and Environmental Research, under contract DE-AC02-06CH113 (to A.J.)

Supporting Information

Procedure for the GBVI/WSA method, an animated .gif image of DapE's conformational flexing, plots for the inactivation of *Hi*DapE by 2,3-butanedione and 2,4,6-trinitrobenzene, and a multiple sequence alignment for DapE proteins supplied as Supporting Information.

References

1. Paphitou, N. I. (2013) Antimicrobial resistance: action to combat the rising microbial challenges. *Int. J. Antimicrob. Agents, 42*, S25-S28.

2. US Department of Health and Human Services (2013) *Antibiotic resistance threats in the United States*, *Atlanta: CDC*.

3. US Department of Health and Human Services (2017) *Antibiotic resistance threats in the United States, Atlanta: CDC*.

4. Fair, R. J.; Tor, Y. (2014) Antibiotics and bacterial resistance in the 21st century. *Perspect Medicin Chem. 6*, 25-64.

5. Gillner, D. M.; Becker, D. P.; Holz, R. C. (2013) Lysine biosynthesis in bacteria: a metallodesuccinylase as a potential antimicrobial target. *JBIC, J. Biol. Inorg. Chem. 18*, 155-163.

6. Karita, M.; Etterbeek, M. L.; Forsyth, M. H.; Tummuru, M. K. R.; Blaser, M. J. (1997) Characterization of Helicobacter pylori dapE and construction of a conditionally lethal dapE mutant. *Infect. Immun. 65*, 4158-4164.

7. Pavelka, M. S., Jr.; Jacobs, W. R.,Jr (1996) Biosynthesis of diaminopimelate, the precursor of lysine and a component of peptidoglycan, is an essential function of Mycobacterium smegmatis. *J. Bacteriol. 178*, 6496-6507.

8. Hutton, C. A.; Perugini, M. A.; Gerrard, J. A. (2007) Inhibition of lysine biosynthesis: An evolving antibiotic strategy. *Mol. BioSyst. 3*, 458-465.

9. Gillner, D. M.; Bienvenue, D. L.; Nocek, B. P.; Joachimiak, A.; Zachary, V.; Bennett, B.; Holz, R. C. (2009) The dapE-encoded N-succinyl-L,L-diaminopimelic acid desuccinylase from Haemophilus influenzae contains two active-site histidine residues. *JBIC, J. Biol. Inorg. Chem. 14*, 1-10.

10. Nocek, B. P.; Gillner, D. M.; Fan, Y.; Holz, R. C.; Joachimiak, A. (2010) Structural Basis for Catalysis by the Mono- and Dimetalated Forms of the dapE-Encoded N-succinyl-L,L-Diaminopimelic Acid Desuccinylase. *J. Mol. Biol. 397*, 617-626.

11. Nocek, B.; Starus, A.; Makowska-Grzyska, M.; Gutierrez, B.; Sanchez, S.; Jedrzejczak, R.; Mack, J. C.; Olsen, K. W.; Joachimiak, A.; Holz, R. C. (2014) The dimerization domain in DapE enzymes is required for catalysis. *PLoS One 9*, e93593/1-e93593/11, 11.

12. Bienvenue, D. L.; Gilner, D. M.; Davis, R. S.; Bennett, B.; Holz, R. C. (2003) Substrate specificity, metal binding properties, and spectroscopic characterization of the DapE-

encoded N-succinyl-L,L-diaminopimelic acid desuccinylase from Haemophilus influenzae. *Biochemistry. 42*, 10756-10763.

13. Reidl, C. T.; Majorek, K. A.; Dang, J.; Law, M.; Tran, D.; Jew, K.; Chiarelli, P.; Minor, W.; Kuhn, M.; Becker, D. P. (2017) PA4794 Gcn5-related N-acetyltransferase bisubstrate inhibitors and mechanistic insights from co-crystal structures, site-directed mutants, and molecular dynamics. *The FASEB Journal. 31*, 923.6-923.6.

14. Starus, A.; Nocek, B.; Bennett, B.; Larrabee, J. A.; Shaw, D. L.; Sae-Lee, W.; Russo, M. T.; Gillner, D. M.; Makowska-Grzyska, M.; Joachimiak, A.; Holz, R. C. (2015) Inhibition of the dapE-Encoded N-Succinyl-L,L-diaminopimelic Acid Desuccinylase from Neisseria meningitidis by L-Captopril. *Biochemistry. 54*, 4834-4844.

15. Lin, Y.; Myhrman, R.; Schrag, M. L.; Gelb, M. H. (1988) Bacterial N-succinyl-L-diaminopimelic acid desuccinylase. Purification, partial characterization and substrate specificity. *J. Biol. Chem. 263*, 1622-1627.

16. Otwinowski, Z.; Minor, W. (1997) Processing of x-ray diffraction data collected in oscillation mode. *Methods Enzymol. 276*, 307-326.

17. Vagin, A.; Teplyakov, A. (2009) Molecular replacement with MOLREP. *Acta Crystallographica Section D: Biological Crystallography. 66*, 22-25.

18. Murshudov, G. N.; Skubák, P.; Lebedev, A. A.; Pannu, N. S.; Steiner, R. A.; Nicholls, R. A.; Winn, M. D.; Long, F.; Vagin, A. A. (2011) REFMAC5 for the refinement of macromolecular crystal structures. *Acta Crystallographica Section D: Biological Crystallography. 67*, 355-367.

19. Adams, P. D.; Afonine, P. V.; BunkÃ³czi, G.; Chen, V. B.; Davis, I. W.; Echols, N.; Headd, J. J.; Hung, L.; Kapral, G. J.; Grosse-Kunstleve, R.; McCoy, A. J.; Moriarty, N. W.; Oeffner, R.; Read, R. J.; Richardson, D. C.; Richardson, J. S.; Terwilliger, T. C.; Zwart, P. H. (2009) PHENIX: a comprehensive Python-based system for macromolecular structure solution. *Acta Crystallographica Section D: Biological Crystallography. 66*, 213-221.

20. Davis, I. W.; Leaver-Fay, A.; Chen, V. B.; Block, J. N.; Kapral, G. J.; Wang, X.; Murray, L. W.; Arendall, W. B.,3rd; Snoeyink, J.; Richardson, J. S.; Richardson, D. C. (2007) MolProbity: all-atom contacts and structure validation for proteins and nucleic acids. *Nucleic Acids Res. 35*, W375-83.

21. Emsley, P.; Cowtan, K. (2004) Coot: model-building tools for molecular graphics. *Acta Crystallogr. , Sect. D: Biol. Crystallogr. D60*, 2126-2132.

22. Molecular Operating Environment (MOE) (2013); Chemical Computing Group Inc., 1010 Sherbooke St. West, Suite #910, Montreal, QC, Canada, H3A 2R7, 2016 .

23. Labute, P. (2008) The generalized Born/volume integral implicit solvent model: estimation of the free energy of hydration using London dispersion instead of atomic surface area. *J. Comput. Chem. 29*, 1693-1698.

24. Born, T. L.; Zheng, R.; Blanchard, J. S. (1998) Hydrolysis of N-succinyl-L,L-diaminopimelic acid by the Haemophilus influenzae dapE-encoded desuccinylase: Metal activation, solvent isotope effects, and kinetic mechanism. *Biochemistry. 37*, 10478-10487.

25. Dutta, D.; Mishra, S. (2016) Structural and mechanistic insight into substrate binding from the conformational dynamics in apo and substrate-bound DapE enzyme. *Phys Chem Chem Phys. 18*, 1671-1680.

26. Harding, M. M. (2006) Small revisions to predicted distances around metal sites in proteins. *Acta Crystallographica Section D: Biological Crystallography. 62*, 678-682.

27. Agarwal, R.; Burley, S. K.; Swaminathan, S. (2007) Structural Analysis of a Ternary Complex of Allantoate Amidohydrolase from Escherichia coli Reveals its Mechanics. *J. Mol. Biol. 368*, 450-463.

28. Botelho, T. O.; Guevara, T.; Marrero, A.; Arede, P.; Fluxa, V. S.; Reymond, J.; Oliveira, D. C.; Gomis-Rueth, F. (2011) Structural and Functional Analyses Reveal That Staphylococcus aureus Antibiotic Resistance Factor HmrA Is a Zinc-dependent Endopeptidase. *J. Biol. Chem. 286*, 25697-25709.

29. Dobritzsch, D.; Gojkovic, Z.; Andersen, B.; Piskur, J. (2003) Crystallization and preliminary x-ray analysis of Î²-alanine synthase from the yeast Saccharomyces kluyveri. *Acta Crystallogr. , Sect. D: Biol. Crystallogr. D59*, 1267-1269.

30. Simon, L.; Goodman, J. M. (2010) Enzyme catalysis by hydrogen bonds: The balance between transition state binding and substrate binding in oxyanion holes. *J. Org. Chem. 75*, 1831-1840.

31. Tang, A. W.; Kong, X.; Terskikh, V.; Wu, G. (2016) Solid-State 17O NMR of Unstable Acyl-Enzyme Intermediates: A Direct Probe of Hydrogen Bonding Interactions in the Oxyanion Hole of Serine Proteases. *J Phys Chem B 120*, 11142-11150.

32. Sievers, F.; Higgins, D. G. (2002) Clustal Omega. In *Current Protocols in Bioinformatics*John Wiley & Sons, Inc.

33. Case, D.; Darden, T.; Cheatham III, T.; Simmerling, C.; Wang, J.; Duke, R.; Luo, R.; Walker, R.; Zhang, W.; Merz, K. (2012) AMBER 12; University of California: San Francisco. 1-826.

34. Gerber, P. R.; Müller, K. (1995) MAB, a generally applicable molecular force field for structure modelling in medicinal chemistry. *J. Comput. Aided Mol. Des. 9*, 251-268.

35. Cosper, N. J.; Bienvenue, D. L.; Shokes, J. E.; Gilner, D. M.; Tsukamoto, T.; Scott, R. A.; Holz, R. C. (2003) The dapE-encoded N-Succinyl-L,L-Diaminopimelic Acid Desuccinylase from Haemophilus influenzae is a Dinuclear Metallohydrolase. *J. Am. Chem. Soc. 125*, 14654-14655.

36. Strater, N.; Lipscomb, W. N. (1995) Transition state analogue L-leucinephosphonic acid bound to bovine lens leucine aminopeptidase: X-ray structure at 1.65 A resolution in a new crystal form. *Biochemistry. 34*, 9200-9210.

37. Dutta, D.; Mishra, S. (2014) The structural and energetic aspects of substrate binding and the mechanism of action of the DapE-encoded N-succinyl-L,L-diaminopimelic acid desuccinylase (DapE) investigated using a hybrid QM/MM method. *Phys. Chem. Chem. Phys. 16*, 26348-26358.

38. Davis, R.; Bienvenue, D.; Swierczek, S. I.; Gilner, D. M.; Rajagopal, L.; Bennett, B.; Holz, R. C. (2006) Kinetic and spectroscopic characterization of the E134A- and E134D-altered dapE-encoded N-succinyl-L,L-diaminopimelic acid desuccinylase from Haemophilus influenzae. *JBIC, Journal of Biological Inorganic Chemistry. 11*, 206-216.

39. Ye, Q.; Xie, S.; Ma, Z.; Huang, M.; Hanzlik, R. P. (2006) Structural basis of catalysis by monometalated methionine aminopeptidase. *Proc. Natl. Acad. Sci. U. S. A. 103*, 9470-9475.

40. Copik, A. J.; Swierczek, S. I.; Lowther, W. T.; D'souza, V. M.; Matthews, B. W.; Holz, R. C. (2003) Kinetic and Spectroscopic Characterization of the H178A Methionyl Aminopeptidase from Escherichia coli. *Biochemistry. 42*, 6283-6292.

41. Holz, R. C. (2002) The aminopeptidase from Aeromonas proteolytica: structure and mechanism of co-catalytic metal centers involved in peptide hydrolysis. *Coord. Chem. Rev. 232*, 5-26.

Table 1. Data Collection and Refinement Statistics.

DATA COLLECTION	
Beamline/Wavelength (Å)	(APS) SBC19-ID / 0.9794
Resolution range	33.48 - 1.95 (2.02 - 1.95)
Space group	I 2 2 2
Unit cell (Å / º)	56.65 135.54 149.61 *90 90 90*
Total reflections	41902
Unique reflections	38497 (2564)
Multiplicity	4.0 (3.2)
Completeness (%)	0.995 (0.997)
Mean I/sigma(I)	16.25 (2.15)
Wilson B-factor	18.02
R_{merge} / R_{meas}	0.10 (0.81) / 0.11(0. 95)
REFINEMENT	
R_{work}/ R_{free}	0.162 (0.179) / 0.184 (0.204)
Bond (Å) /Angles (º)	0.008 / 1.174
Number of non-hydrogen atoms	3191
macromolecules	2936
ligands	23
Protein residues	384
RMS(bonds)	0.008
RMS(angles)	1.13
Ramachandran favored / allowed (%)	98 / 2.1
Ramachandran outliers (%)	0
Rotamer outliers (%)	2.2
Clashscore	0.85
Average B-factor (Å^2)	25.99
Molecule / Ligands / Solvent (Å^2)	25.66 /20.39 / 30.69

Statistics for the highest-resolution shell are shown in parentheses.